Chemical Physics Letters 662 (2016) 137–140

Contents lists available at ScienceDirect

Chemical Physics Letters

journal homepage: www.elsevier.com/locate/cplett

Research paper

Experimental study on capillary filling in nanochannels

Min Yang (杨敏)[a,b], Bing-Yang Cao (曹炳阳)[b,*], Wei Wang (王玮)[c,*], He-Ming Yun (云和明)[a], Bao-Ming Chen (陈宝明)[a]

[a] Key Laboratory of Renewable Energy Utilization Technologies in Buildings of the National Education Ministry, Shandong Jianzhu University, Jinan 250014, China
[b] Key Laboratory for Thermal Science and Power Engineering of Ministry of Education, Tsinghua University, Beijing 100084, China
[c] National Key Laboratory of Science and Technology on Micro/Nano Fabrication, Peking University, Beijing 100084, China

ARTICLE INFO

Article history:
Received 18 July 2016
In final form 10 September 2016
Available online 12 September 2016

ABSTRACT

We investigated the capillary filling kinetics of deionized water in nanochannels with heights of 50–120 nm. The measured position of the moving meniscus was proportional to the square root of time, as predicted by the LW equation. However, the extracted slopes were significantly smaller than the predictions based on the bulk properties. This unusual behavior was found to be mainly caused by the electro-viscous effect and dynamic contact angle, which was significantly larger than the static angle. In addition, when the filling distance reached about 600 μm, bubbles tended to be formed, leading to the main meniscus was almost immobile.

With the rapid development of micro- and nanotechnologies over the past twenty years, capillary filling kinetics in micro- and nanochannels has become one of the most important topics because of its significant effects on oil recovery, design of micro- and nanofluidic devices, fabrication of nanostructured materials, etc. [1–4]. Almost a century ago, the capillary filling kinetics of Newtonian liquids in a small cylindrical tube was first investigated by Lucas [5] and Washburn [6]. The penetrating length $l(t)$ was found to be linearly proportional to the square root of time $t^{1/2}$, known as Lucas-Washburn (LW) equation

$$l(t) = \left(\frac{\sigma_{LV} R \cos\theta_e}{2\eta}\right)^{1/2} \sqrt{t} \tag{1}$$

where σ_{LV} is the surface tension coefficient at liquid-air interface, η is the dynamic viscosity of liquid phase, R is the tube radius and θ_e is the equilibrium contact angle. Although the LW equation has been widely verified by macroscale experiments [5], its availability at micro- and nanoscale remains an open question [7–9]. Several groups [10–15] have experimentally investigated liquid filling processes in micro- and nanochannels and found that the filling kinetics obeyed the expected $\sqrt{t}$-dependence according to the LW equation. However, significant deviation was observed between experimental filling speeds and the theoretical expectations. While several possible factors have been used to explain the deviation, such as the electro-viscous effect, increased filling resistance, the dynamic contact angle effect, there still lacks a clarified understanding of the underlying mechanism.

The aim of the present work is to capture the key points in the capillary filling kinetics at nanoscale based on an experimental investigation using nanochannels with different heights. For all the cases, the filling kinetics followed the expected $\sqrt{t}$-dependence, which was in accordance with the LW equation. While the filling speed was significantly lower than the expected values. The electro-viscous effect and dynamic contact angle were demonstrated to be responsible for the deviation.

The nanochannels with a rectangular cross section used in our experiments were fabricated by the triple thermal oxidation and silicon-glass anodic bonding developed by our own group [16]. Fig. 1 shows the fabrication process of nanochannels with the following procedures: (a) A SiO_2 layer of d_1 thickness was firstly thermally grown on the silicon substrate; (b) The pattern of nanochannels was then defined by a lithography process; (c) The second oxidation was conducted to grow a SiO_2 layer of d_2 thickness in the nanochannel region and an oxide layer of d_3 thickness in the non-nanochannel region because of the diffusion of oxygen molecules; (d) A nanochannel with a height of h was finally obtained after etching all oxide layers on the substrate; (e) Electrical insulation was ensured by the third oxidation, whereas the nanochannel height remained h due to the uniformity of the thermal oxidation process; (f) Enclosed nanofluidic channels were formed by silicon-glass anodic bonding. A cross-sectional scanning electron microscope image of the fabricated nanochannel with a height of 50.6 nm is presented in Fig. 2. It is seen that the enclosed nanofluidic channel has a uniform cross-section and the silicon-glass anodic bonding is effective.

* Corresponding authors.
E-mail addresses: caoby@tsinghua.edu.cn (B.-Y. Cao), w.wang@pku.edu.cn (W. Wang).

http://dx.doi.org/10.1016/j.cplett.2016.09.016
0009-2614/

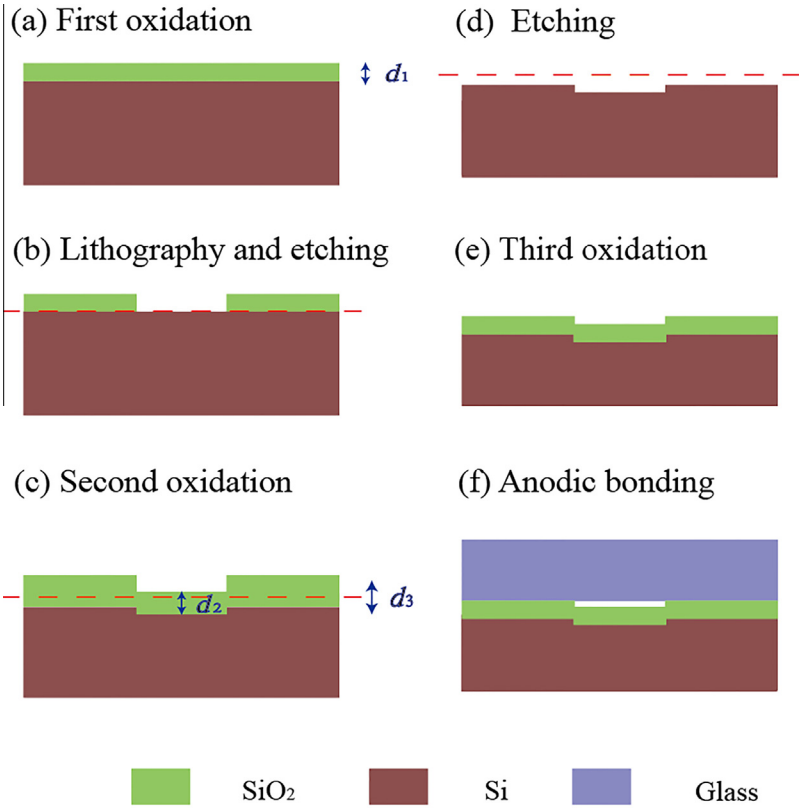

Fig. 1. Schematic of the nanochannel fabrication process.

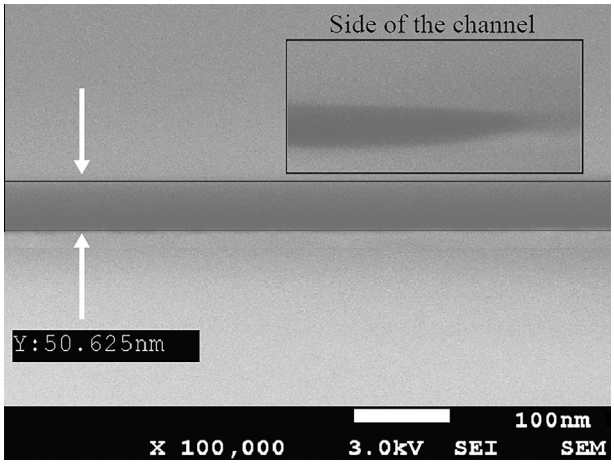

Fig. 2. SEM image of the cross-section of nanochannel with height of 50.6 nm. The inset shows the side of the fabricated nanochannel.

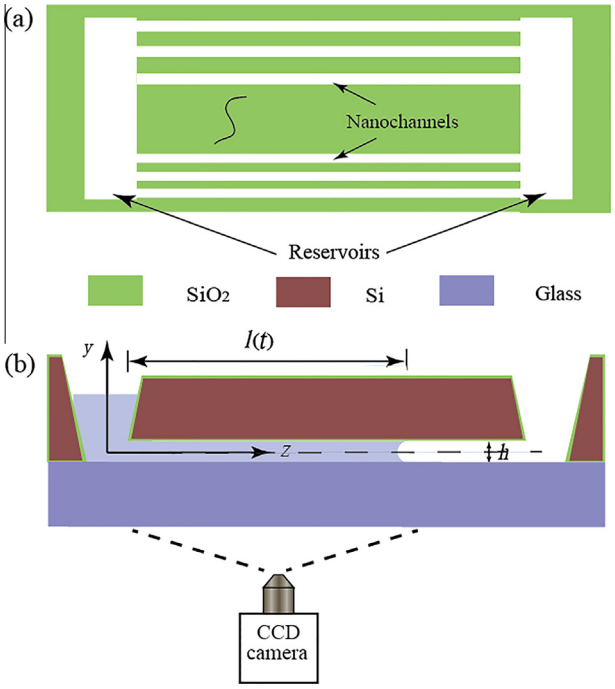

Fig. 3. Schematic illustration of (a) the layout of the nanofluidic chip and (b) capillary filling process in a nanochannel with height *h*.

Fig. 3(a) shows the layout of the nanofluidic chip. The heights of the fabricated nanochannels are respectively 50.6 nm, 65.6 nm, 75.0 nm and 114.8 nm. The nanochannels were fabricated with different widths to check their influence, which was found to have negligible effect on the filling process because of an extremely small height-width ratio. The schematic of the experimental apparatus is shown in Fig. 3(b). To measure the position of the meniscus as a function of time at room temperature, a drop of 10 μL deionized water was deposited onto the reservoir area. Once the droplet arrived at the inlet of the nanochannel, the filling process of the liquid began due to capillary force and could be observed by our microscope (Axio Vert.A1 from Zeiss). A high speed digital camera (ProgRes SpeedXT core5, resolution: 1394/2580 × 1944 pixels) was used to visualize the liquid filling process and track the position of the meniscus. Fig. 4 displays sequences of the images of the water filling in nanochannels with a height of 50.6 nm, where the filled

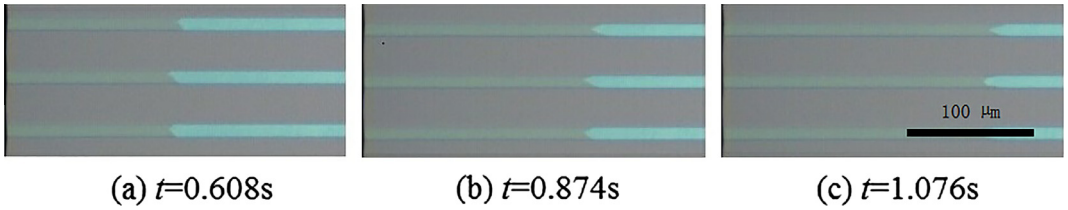

Fig. 4. The images of capillary filling of deionized water in nanochannels at different moments. (a) t = 0.608 s; (b) t = 0.874 s; (c) t = 1.076 s.

part of the channels appears darker. In addition, when the capillary filling distance reached about 600 μm, bubbles tended to be formed at the liquid front, which could make the meniscus unclear. Therefore, measurements of the filling position as a function of time were carried out before large bubbles started to form. The recorded images were then analyzed using the ProgRes CapturePro software.

For a rectangular cross-section channel with an extremely small ratio of the channel height h to the width w, the LW equation can be described as [10]

$$l(t) = \left(\frac{\sigma_{LV} h \cos\theta_e}{3\eta}\right)^{1/2} \sqrt{t} = A\sqrt{t} \tag{2}$$

where h is the channel height and A is the LW coefficient. Fig. 5 shows the measured position $l(t)$ of the advancing meniscus as a function of the square root of time. Each datum point is averaged from three independent filling experiments in order to reduce the error. For all the channels we tested, the position of the advancing meniscus was observed to be approximately linearly proportional to the square root of time $t^{1/2}$, and the filling speed decreased with the decreasing channel height, which was in accordance with the modified LW equation, Eq. (2). However, the extracted slopes through linear fitting (i.e. the LW coefficient A) for the four cases were respectively 23.3%, 30.8%, 34.9% and 36.1% of the macroscopic expectations based on the bulk properties, as shown in Table 1. In addition, A_{exp} was closer to A_{LW} when the channel became deeper, which indicated that the size effect on the filling process decreased.

Possible explanations should be considered for the observed reduced filling speed than the expectations: surface roughness effects, stagnant layers due to liquid-wall interaction, electro-viscous effect, and dynamic contact angle effect. Owing to the size effect, the surface roughness could possibly have great influence on the capillary filling in nanochannels, such as enhancing the filling resistance and decreasing the effective height of channels. The

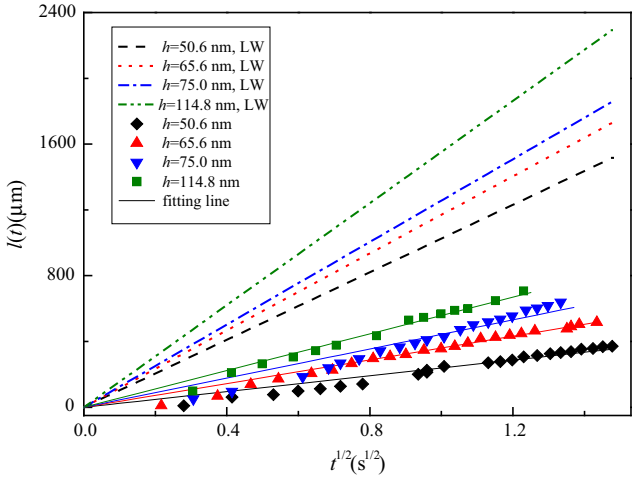

Fig. 5. Schematic of the position of moving meniscus versus time.

Table 1
The LW coefficients for capillary kinetics of deionized water in nanochannels with different heights.

Height (nm)	A_{exp} (μm/s$^{1/2}$)	A_{LW} (μm/s$^{1/2}$)	A_{exp}/A_{LW}
50.6	239	1026	0.233
65.6	360	1170	0.308
75.0	440	1258	0.349
114.8	560	1551	0.361

mean surface roughness of the nanochannel bottom was measured by tapping mode AFM over a surface area of 2.5 μm × 2.5 μm and had a value of 0.229 nm [16], much smaller than the channel height. Another possible factor that may influence the filling process is the stagnant water layers on the solid surface due to the strong liquid-wall interaction, which can reduce the effective height of the channel by about two molecular diameters (about 0.8 nm for water) [17]. Nevertheless, it has been found previously that both the surface roughness and the stagnant water layers have only a very minor influence on the filling kinetics and can be ignored [18]. Another factor which should be taken into account is the electro-viscous effect. The interfacial charged properties, such as electric double layers effect and the Stern layer, are important for ionic transport behavior within nanochannels [19–22] and the electro-viscous effect is caused by the presence of the electrical double layer near the wall-liquid interface [10,23]. The electro-viscous effect can increase the apparent dynamic viscosity due to the electro-osmotic counter flow induced by a streaming potential. Following the theory of Mortensen and Kristensen [23], the ratio of apparent to bulk dynamic viscosity is given by

$$\frac{\eta_{EDL}}{\eta} = 1 + 12\left(\frac{k}{h}\right)^4 \left(\frac{\frac{h}{k} - 2 + \left(\frac{h}{k} + 2\right)e^{-h/k}}{1 + e^{-h/k}}\right)^2 \chi \tag{3}$$

and $\chi = \frac{\varepsilon\zeta^2}{\eta D}$ expresses the square of the ratio between the electro-osmotic mobility and the viscous mobility, where η_{EDL} is the apparent dynamic viscosity, η is the bulk dynamic viscosity, k^{-1} is the Debye length, h is the channel height, ε is the dielectric function of the liquid, ζ is the zeta potential and D is the diffusion coefficient of ions. With the aid of bulk properties of water (T = 293 K, η = 1.005 cP, σ_{LV} = 0.073 N/m, k^{-1} = 200 nm [10,19], ζ = −86 mV [24–26]), the calculated apparent viscosity for the four channels was respectively 3.2%, 5.4%, 7.1% and 16.2% higher than the bulk viscosity. The enhanced viscosity due to the electrokinetic effect thus appreciably increased the filling resistance and the recalculated values of A_{exp}/A_{LW} for the four channels were respectively 0.230, 0.342, 0.414 and 0.506. Therefore, considering only the electro-viscous effect is insufficient to explain the significant deviation between the experimental filling speed and the expectation based on the LW equation, which is consistent with Refs. [7,23].

To adequately explain the anomalous experimental results, the dynamic contact angle (i.e. θ_D) must be taken into account. The usual dynamic contact angle is actually an equilibrium one measured on a flat surface subject to measurement techniques in confined space, which may limit our understanding of capillary filling

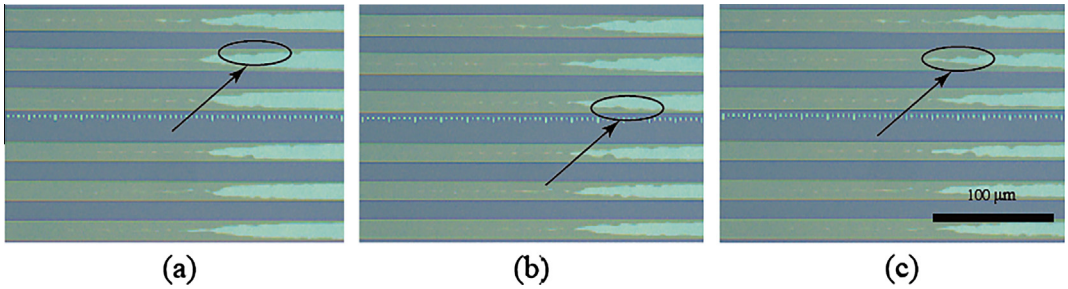

Fig. 6. Bubble trapping process. Time between images: 0.5 s. The narrows in all images indicate the liquid wetting along two sides and the trapped bubbles.

kinetics [27]. Recent work has demonstrated that θ_D alters due to different factors and several dynamic contact angle models have been proposed [28–32]. As is well known that liquid flow at micro- and nanoscale much differs from its macroscopic counterpart thanks to the great size effect. Therefore, those models cannot be adapted to the present work as they neglect the key characteristics of capillary filling in micro- and nanochannels. Some researches [11–13] directly extracted θ_D of capillary filling process in nanochannels by inserting the fitted A values and liquid bulk properties into the LW equation. The results we obtained were in accordance with the LW equation, i.e. the $l(t)$–$t^{1/2}$ scaling law, which implied that the dynamic contact angle remained independent of time for each case in our experiments. Schwartz and Tejada [33] pointed out that the dynamic contact angle behavior can be divided into three regions based on the capillary number Ca: (I) $Ca < 2 \times 10^{-6}$, θ_D is approximately constant; (II) $10^{-6} < Ca < 2 \times 10^{-3}$, θ_D rapidly increases with Ca; (III) Ca is higher than a specified value ranging from 5×10^{-4} to 5×10^{-3}, θ_D slowly increases with Ca. In the present work, the calculated Ca (in the range of $0.5–20 \times 10^{-6}$) is in region II during the early stage of capillary filling and in region I in the later stage of capillary filling, which infers that θ_D rapidly increases in an extremely short initial period and then approximately approaches a constant. Thus we obtained the dynamic contact angle from the fitted A values and the bulk properties of liquid based on the LW equation, considering also the correction from the electro-viscous effect. The dynamic contact angles of the four channels were respectively 87°, 84°, 80° and 73°, significantly larger than the equilibrium contact angle (about 30°). The results clearly indicated that the contact angle would significantly increase when water filled into the nanochannels, resulting in a decrease of the contact line moving speed. Moreover, the dynamic contact angle became closer to the equilibrium one when the channel was deeper, indicative of a decreased size effect on the filling process.

In addition, it is obvious that small air bubbles were formed by enclosure of air as shown in Fig. 6. The presence of bubbles is a common phenomenon in capillarity-driven filling of micro- and nanofluidic channels [10–12,14,15]. We observed an interesting phenomenon that when the capillarity-driven filling distance reached about 600 μm, the corner flow (water filled along the two lateral sides of the channel) spread in front of the main meniscus, which led to the enclosure of air and the formation of bubbles (Fig. 6). The presence of big bubbles can make the main meniscus almost immobile. We measured the position of the meniscus as a function of time before large bubbles formed so that the presence of air bubbles has only a very minor influence on the filling kinetics and can be ignored.

In conclusion, we measured the capillary filling kinetics of deionized water in nanochannels with heights of 50.6 nm, 65.6 nm, 75.0 nm and 114.8 nm. The position of the moving meniscus increased linearly with the square root of time, which agreed with the classical LW equation. The extracted slopes by linear fitting for the four channels were respectively 23.3%, 30.8%, 34.9% and 36.1% of the expected values based on the bulk properties. We conclude that the dynamic contact angle is the main reason for the deviations at naonoscale, and can explain well the experimental results combining with the electro-viscous effect. For all the cases, the dynamic contact angle approached approximately constant values, which were respectively 87°, 84°, 80° and 73°, significantly larger than the equilibrium value (about 30°). In addition, when the filling distance reached about 600 μm, the main meniscus was nearly immobile, which was resulted from bubbles formation in the capillary filling process.

Acknowledgment

This work is financially supported by Foundation of Key Laboratory of Renewable Energy Utilization Technologies in Buildings of the National Education Ministry in Shandong Jianzhu University and the National Natural Science Foundation of China (Grant Nos. 51322603 and 91323304).

References

[1] C. Jian-Chao et al., Chin. Phys. Lett. 27 (2010) 054701.
[2] W. Tian et al., Nanoscale 3 (2011) 4094.
[3] B.Y. Cao et al., Polymer 52 (2011) 1711.
[4] B.Y. Cao, M. Yang, G.J. Hu, RSC Adv. 6 (2016) 7553.
[5] R. Lucas, Kolloid Z. 23 (1918) 15.
[6] E.W. Washburn, Phys. Rev. 17 (1921) 273.
[7] V.N. Phan, C. Yang, N.T. Nguyen, Microfluid. Nanofluid. 7 (2009) 519.
[8] N. Fries, M. Dreyer, J. Colloid Interfaces Sci. 320 (2008) 259.
[9] A.V. Pesse, G.R. Warrier, V.K. Dhir, Int. J. Heat Mass Transfer 48 (2005) 5150.
[10] N.R. Tas et al., Appl. Phys. Lett. 75 (2004) 3274.
[11] A. Han et al., J. Colloid Interfaces Sci. 293 (2006) 151.
[12] M.N. Hamblin et al., Biomicrofluidics 5 (2011) 1359.
[13] Y. Zhu, K. Petkovic-Duran, Microfluid. Nanofluid. 8 (2010) 275.
[14] J. Haneveld et al., J. Appl. Phys. 104 (2008) 14309.
[15] K.M. van Delft et al., Nano Lett. 7 (2007) 345.
[16] Y.W. Ou, W. Wang, Biomicrofluidics 8 (2014) 5216.
[17] J.M. Oh et al., Microfluid. Nanofluid. 9 (2010) 123.
[18] B.Y. Cao, M. Chen, Z.Y. Guo, Phys. Rev. E 6 (2006) 066311.
[19] Y. Ma et al., Phys. Chem. Chem. Phys. 16 (2014) 20138.
[20] C. Duan, A. Majumdar, Nat. Nanotechnol. 5 (2010) 848.
[21] Y. Kazoe et al., Anal. Chem. 83 (2011) 8152.
[22] W. Guan et al., Lab Chip 13 (2013) 431.
[23] N.A. Mortensen, A. Kristensen, Appl. Phys. Lett. 92 (2008) 063110.
[24] D. Erickson, D. Li, C. Werner, J. Colloid Interfaces Sci. 232 (2000) 186.
[25] M. Taghipoor, A. Bertsch, P. Renaud, Phys. Chem. Chem. Phys. 17 (2015) 4160.
[26] Y. Ma et al., Anal. Chem. 87 (2015) 4508.
[27] X. Li et al., Chem. Eng. Sci. 117 (2014) 137.
[28] M.N. Popescu, J. Ralston, R. Sedev, et al., Langmuir 24 (2008) 12710.
[29] R.G. Cox, J. Fluid Mech. 168 (1986) 169.
[30] T.D. Blake, J.M. Haynes, J. Colloid Interfaces Sci. 30 (1969) 421.
[31] T.S. Jiang, O.H. Soo-Gun, J.C. Slattery, J. Colloid Interfaces Sci. 69 (1979) 74.
[32] M. Bracke, F. De Voeght, P. Joos, Prog. Colloid Polym. Sci. 79 (1989) 142.
[33] A.M. Schwartz, S.B. Tejada, J. Colloid Interfaces Sci. 38 (1972) 359.